2-Dimentional Bipedal Passive-Dynamics Based Walker
Marathon Walker Project
Foot & Tensioner Design
Biorobotics and Locomotion Laboratory

M&AE 491 Senior Design Project – 5 credits

Zim Harry

38-01 112th Street Apt. 7B
Corona, NY 11368
Phone: (607) 280-1538
email: zh23@cornell.edu

May 13, 2005

Abstract

I implemented a new foot movement system and designed and installed new feet on an existing, but non-functional walking robot. The overall system objective was to utilize retrofitting to enhance the walker robot's endurance, robustness and efficiency of gait .

1 Introduction

The purpose of this design project was to retrofit novel features onto an older design, thereby enabling the older design to meet newly established criterion on endurance, robustness, and efficiency in walking. The design, fabrication and implementation of the robotic feet and tensioners for the feet drive belts were placed in my charge. The design and implementation of the retrofitted components were iterative processes that will later be discussed in detail.

Figure 1 – 2D bipedal walker

During the summer of 1998, Larry Gosse (M.Eng 1998) and Yan Yevmenenko fabricated what is our current, 2-dimetional passive dynamic based walker. The mechanism under study is a straight-legged walker with articulating circular feet that are powered by ankle torques [Yevmenenko, 2000] It is presumed that the 1998 group selected circular feet for the walker to simplify the modeling and simulation process. Work on the 2-dimentional passive dynamic walker was continued on by Oren B. Yeshua, Joshua Silbermann, and Mario Gomes in 2003. The previous design saw little mechanical improvement as this group saw a greater need in implementing better software control. The mechanical improvements implemented by this group included the addition of an Infrared (IR) switch mounted to a wooden arc on the outward facing portion of the inner leg. While the goal is to walk with a minimal amount of control, some feedback from the walker is necessary in order to determine when to rotate each of the ankles and to control their position. [Yeshua, 2003] The 2003 group perceived the IR switch as a solution to this problem. Additionally, separation problems with the rubber attached to the bottoms of the circular feet were duly noted by the 2003 group and solved utilizing rubber sleeves and rubber to metal epoxy.

2 Methods & Results

My first viable foot design occurred after three iterations. It incorporated a curve of arbitrary radius of curvature (as opposed to a more square heel-toe profile) at the bottom of the foot to reduce jerkyness of the heel to toe of transition in walking. The final design of the foot was reached after 6 successive refinements to the original conceptual foot design (refer to appendix for the first three iterations). The drive belt tensioner final design was obtained only through one iteration.

2.1 Solution Synthesis

The development of the foot design will be discussed followed by the design for the tensionsers. This discussion begins with the fourth iteration of the foot design.

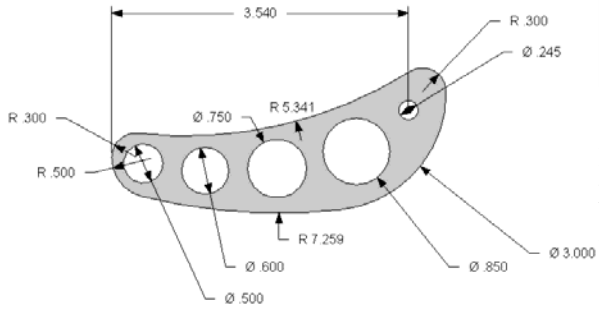

Figure 2 – Iteration #4

A rounded heel was introduced in iteration 4 to increase the available heel strike surface. The new placement of the ankle axis ensured that the foot can rotate to a position parallel to the walker's legs during leg transitions and remain flush with base of the leg and 0.8-inches from the ground (see figure 3). The foot clearance remains essentially the same during the ensuing foot design iterations.

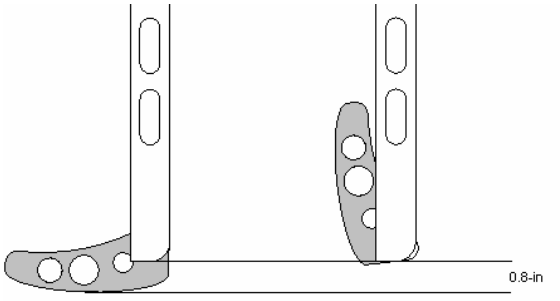

Figure 3 - Foot clearance diagram of final foot design (0.8-inches clearance from ground when foot extended 90-degrees to leg)

However, this design (iteration #4), like the first three was impractical. The incorporation of curves with different radii of curvature, 0.5-inches, 7.259-inches, and 3.000-inches from the toe to the heel respectively proved to be non-trivial for dynamics modeling.

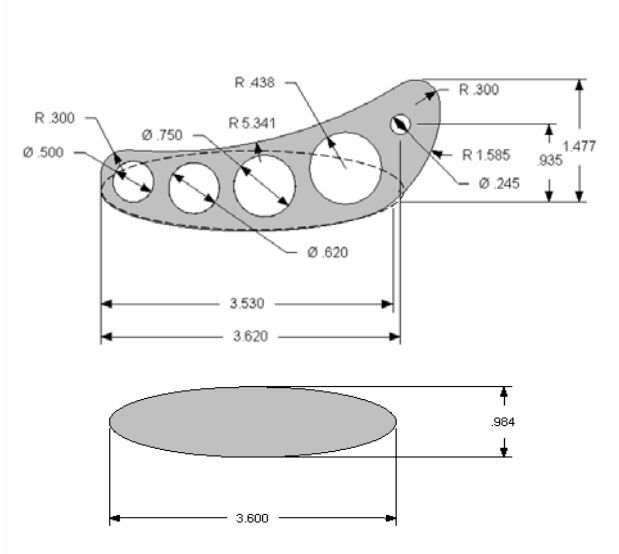

Figure 4 – Iteration #5

Design iteration #5 incorporates aspects of the previous four iterations. However, this design is a simplifying improvement upon iteration #4. Rather than the three curves of differing radii of curvature at the bottom of the foot, there is just one curve, an elliptical curve, which has a major axis of length 3.6-inches and extends from the toe to an area just behind the heel (0.090-inches). The position of the heel of the foot is measured to be 3.530-inches from the toe.

2.2 Experimental Analysis

In order to proceed further with the proposed solution, it was necessary to perform calculations to assure that the design was feasible from a technical standpoint. It was assumed that the foot actuation motors installed on the walker robot will not be modified or changed during the retrofit process. Considering this fact, the following experiment concerning the foot actuation motors are now relevant.

2.3 Motor Analysis

Motor Model: *Foulhaber Motor Shönaich* 3042W012C (Micro MO Electronics)

The objective of this analysis is to find the maximum toe-off torque given the current motor and its 29:1 gearing ratio. The experiment proceeds as follows:

The onboard battery indicated a measured 12.5V charge at the onset of this test. The motors currently installed on the robot are rated for 12V. Next a wooden beam was attached securely to a foot along with three Triple Beam Balance weights weighing 295g, 295g, and 147.5g. Since the wooden beam could not be considered near massless, it was considered to be a distributed load with resultant force located at the middle. The motor was powered on and serendipitously was near stall torque under the described loading.

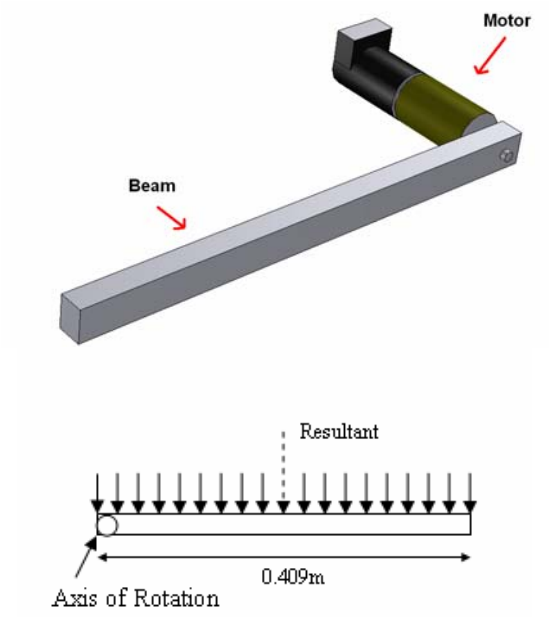

Figure 5 – Foot torque testing beam. Due to the direct drive setup between the motor and the feet, the motor torque experiment diagram can be simplified as a beam directly connected to the motor shaft.

Taking into account the 737.5g total mass at the end of the wooden beam, the magnitude of the reaction torque provided by the motor at the foot can be found.

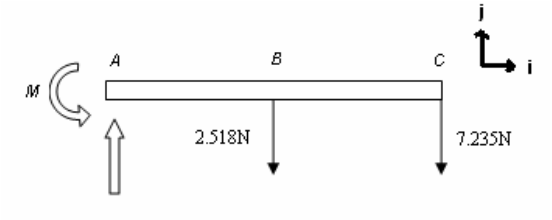

Figure 6 – Free body diagram of foot torque testing beam where 2.518N is the beam resultant force, 7.235N is the force of the end mass and M is the unknown foot reaction torque.

Starting with the sum of the moments about point A in figure 6 the result is the following

$$\sum M_A : r_{B/A} \times F_B + r_{C/A} \times F_C - M = 0$$

where $r_{B/A}$ is the moment arm of F_B (force at point B) with respect to A and likewise $r_{C/A}$ is the moment arm of F_C (force at point C) with respect to A. The lengths of the moment arms $r_{B/A}$ and $r_{C/A}$ are 0.205m and 0.406m, respectively. Thus the reaction moment M is

$$\sum M_A : (0.205m\vec{i}) \times (-2.518N\vec{j}) + (0.406m\vec{i}) \times (-7.235N\vec{j}) - M = 0$$

$$M = 3.454Nm\vec{k}$$

Maximum Toe-off Force Calculations:
Length of foot from axis of rotation:
3.615 in = 0.092 m
Torque (M): 3.454Nm

Maximum force at toe-off:

$$\frac{3.454Nm}{0.092m} = 37.5N$$

Total Robot mass: 16.5-lbs = 7.484-kg = 73.421N

According to design requirements, the maximum toe-off force (i.e. the maximum sustainable force at the toe) must be at least half the total weight of the walker. Since the half the total weight of the walker is 36.71N, the design meets this requirement within experimental error. The chief mode for error in this experiment was that the motor was near stall, not at stall.

2.4 Design Description

In this section, the final designs of both the newly installed feet and belt tensioners will be discussed.

2.5 Foot Design

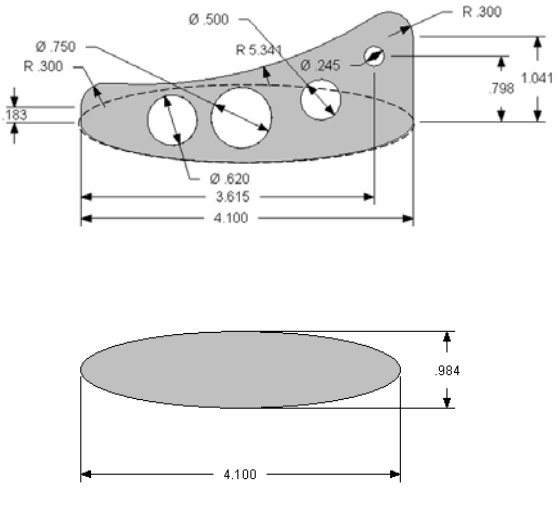

Figure 7 – Final foot design

The final design further simplifies the design of iteration #5 while maintaining aspects of its functionality. The changes to iteration #5 include removal of the toe hole, the shrinking of the heel hole to accommodate the placement of limit switches, and the removal of the curved heel. The 1.585-inch radius heel was removed in favor of a lengthened sole defined by an elliptical curve because it is more electrically efficient to have a foot that experiences no torques on the ankle shaft during heel strike. Toques on the ankle shaft during heel strike may cause the foot motors to stall, forcing the motors to consume a great deal of energy over a short period of time. The elliptical curve characterizing the sole of the foot had a major axis of 4.1-inches and minor axis of 0.985-inches defined by the following equation:

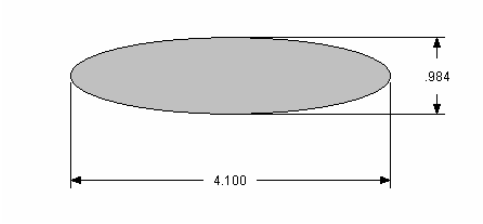

$$y = \pm\sqrt{\left(1 - \frac{x^2}{4.025}\right)(0.2421)}$$

Figure 8 – Equation governing the foot ellipse. In particular, it is the negative form of this equation that defines the underside of the foot.

Such an elliptical curve was selected due to constraints on the length of the foot. As previously discussed, the length of the foot cannot be extended much more than 3.615-inches from the ankle axis to the toe otherwise the maximum output torques of the walker's installed *Foulhaber* motors may be exceeded. The length of the foot must also not be excessive past the defined ankle to ensure that clearance tolerances are not surpassed.

2.6 Tensioner Design

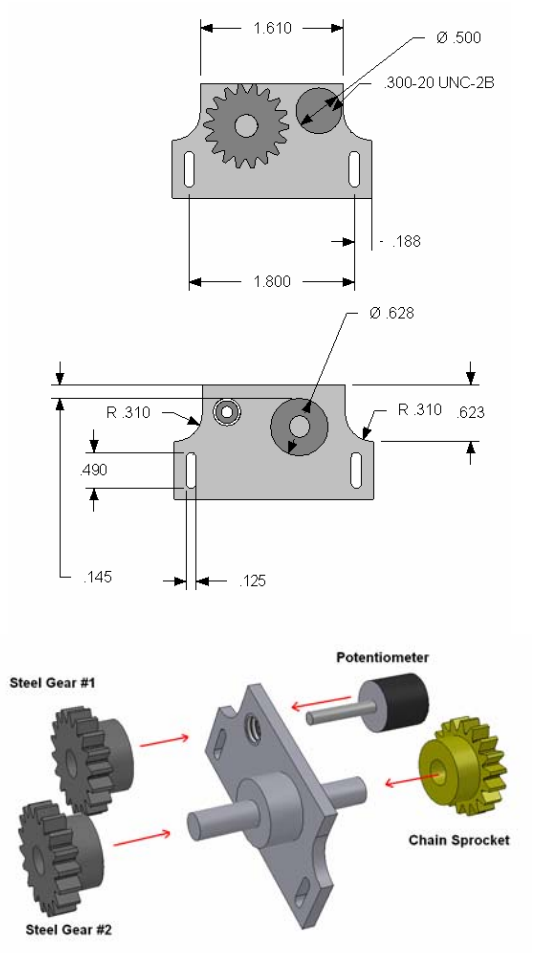

Figure 9 – Tensioner final design

The chain tensioner for the walker was designed for two purposes. Its primary function is to apply adjustable tension to each of the three sprocket belts and secondly it was meant to be a structure upon which potentiometers would be secured to read the positions of the feet at any given time. This design involved the usage of a chain sprocket which would have some angular displacement directly corresponding to any movements of the belt (see figure 9). This movement is then simultaneously transmitted to steel gear #2 which turns steel gear #1, which is directly fixed to the potentiometer shaft. Hence, any angular translation of the belt sprocket leads to a corresponding angular translation of the potentiometer shaft. This design was selected over an in-line design with a soft connection to the potentiometer shaft since the soft connection will have a tendency to slip and flex as the belt moved, thereby decreasing the accuracy of foot position readings. In the end, our group resorted to utilizing the potentiometers over the optical encoders installed on the *Foulhaber* motors because the *Foulhaber* motors possessed incredibly fine encoder resolutions. At 500 clicks per revolution, the resolutions were too fine for our Innovation First robot controller to read effectively. It was determined that the Innovation First controller can only read the encoders properly if most of its processing power were allocated to counting. This was not an option since the controller had to process readings from the foot limit switches and respond with an appropriate movement quickly.

2.7 Considerations for Construction

To ensure the timely production of components, the foot and tensioner designs were altered from their original dimensional specifications to take into account available tooling and to reduce the number of machining steps.

Component	Quantity	Number of Machining Steps per Component	Number of Machining Hours per Component
Foot	4	12	3.5
Tensioner	3	11	1.5

Machining steps included cutting, drilling and filing. Polishing was not included as a machining step, but was approximately 10 minutes per part.

2.7.1 Foot Considerations

The initial foot design did not take into account readily available tooling at Emerson Fabrication Laboratory. Some tools were broken or difficult to find. Starting with arbitrary sizes, all hole diameters in the feet were readjusted to fit available tooling, thus all hole diameters were rounded up or down to the nearest appropriate drill bit diameter.

Tool	Size
Drill Bit	0.25″ Diameter
Drill Bit	0.620″ Diameter (11/16)
Drill Bit	0.75″ Diameter
Drill Bit	0.5″ Diameter

The final foot design minimizes the number of complicated machining steps that previous design iterations yielded by removing the 1.585-inch radius heel curve and replacing it with a straight heel. Due to the thinness of the aluminum stock, from which the feet were produced, I had some reservations in drilling through the top of the foot.

Therefore, a friction lock (see figure 10) was initially conceived to secure the feet to their respective ankle shafts. However, I later found that this was not a truly secure method, so set pins were subsequently incorporated into the feet.

2.7.2 Tensioner Considerations

The tensioner is constructed of a rectangular aluminum plate with a width of 2.170-inches and a length of 1.360-inches (see figure 9).

Tool	Size
Endmill	0.25″ Diameter (for slots)
Endmill	0.620″ Diameter (for fillets)
Drill Bit	0.620″ Diameter
Drill Bit	0.25″ Diameter

Small fillets were placed on both sides of the tensioner for aesthetic purposes, though a minor weight reduction also resulted. Two elongated slots were placed in the tensioner design to ensure adjustability of belt tension. The movable components on the tensioner include a shaft on two flanged bearings (see Bill of Parts) and two steel gears for transmission of torque from the belt sprocket to the potentiometer. The gears were duly adjusted to ensure that the potentiometer rotational limits were not encountered during normal belt and foot movements.

3 Discussion

During the course of the design and implementation of the retrofit regime for the robotic walker, some difficulties occurred in the implementation of the foot and tensioner designs. These anomalies will be discussed within this section.

3.1 Foot

Due to the thinness of the foot stock (0.125”) it was originally intended that a cylindrical clamp (friction lock) be secured to each foot’s serrated ankle hub and the foot itself subsequently installed upon a steel ankle shaft.

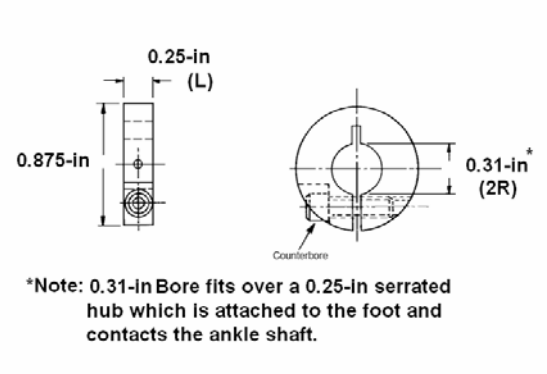

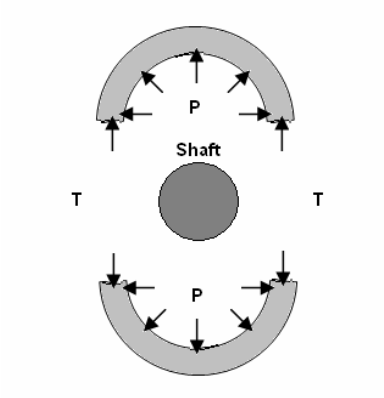

$$\sum F_x = 0$$

$$\sum F_y : 2\pi RLP - 2T = 0$$

$$P = \frac{T}{\pi RL}$$

Figure 10 – Engineering schematic and freebody diagram of split hub clamp. In the free body diagram L is the thickness of the hub into the page.

Accordingly, to find the friction toques due to the clamp, one must take the product of shear along the surface of the shaft, the surface area of the clamping region on the shaft (2 X 0.1964-sq. in) and the radius of the shaft (0.125”), thus

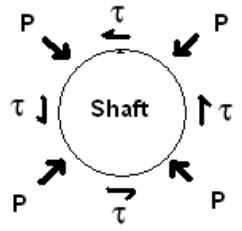

$$M = \tau A_S R$$

where shear force, τ is the product of the clamp pressure, P on the shaft and the coefficient of static friction, μ_S on the shaft. A steel on steel interface is involved in the clamping action, therefore according to [Baumeister, .et al, p. 3-26 Table 1] the coefficient of static friction in a steel on steel interface is 0.78. Hence, using the following equation

$$M = 2\mu_S TR$$

where T is the product of the yield stress of annealed stainless steel (38,000-lb/in^2 ~ $2.62\times10^8\,Pa$) [Beer & Johnston, p 700] and the cross sectional area of the screw applying tension to the clamp. Using this formulation, the maximum torque the steel on steel interface can sustain is

$$M = 2\mu_S TR$$
$$M = 2(0.78)(2.62\times10^8\,Pa)(9.23\times10^{-6}\,m^2)(0.00318m)$$
$$M = 11.98Nm$$

This value reflects the sustained clamping pressure encountered if the steel screw was tightened to yield. However, for all practical purposes, the screw was only tightened to a fraction of yield since the steel on steel clamp interface still slipped around the ankle axis in practical tests (albeit with relative difficulty). However, it should be noted that the force of the robot's weight directed through the legs and any forces due to impact of the feet produce torques on the robot ankle that oppose the motor toque, thus aggravating slippage along the ankle shaft. This is probably the main reason why the friction torque value aforementioned was exceeded. A sturdier means of foot attachment was necessary to counteract the slippage under these various ankle torques.

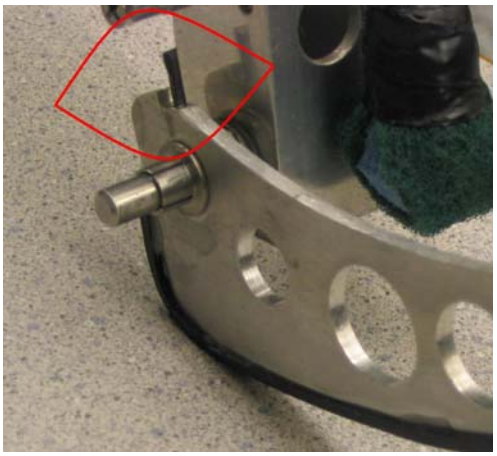

Figure 11 – Circled area shows spring pin inserted through the top of a foot into an ankle shaft

The solution was to drill a $\frac{3}{32}$ inch hole through the top of the foot and insert the same sized hardened steel spring pin through the foot into the ankle shaft. This solution ensured a steadfast hold of the foot to the ankle shaft under the design loads foreseen and additional strength to accommodate the ever increasing weight of the passive- dynamic based walker.

A secondary problem that occurred with the newly installed feet was a tendency for the rubber soles to shear off the foot. A likely cause for these separations would be shear stresses between the bottom of the foot, the rubber soles and the ground, augmented by the imperfect attachment of the rubber sole to the bottom of the foot with a general purpose epoxy. Hence, a simple investigation was executed to circumvent this issue.

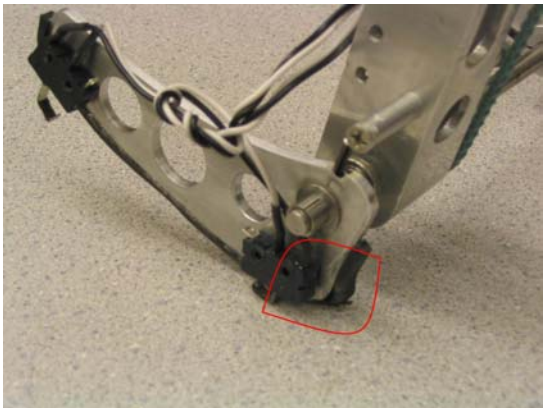

Figure 12 – Circled area shows rubber separation at heel

A qualitative test using three different adhesives was performed with a piece alcohol-treated aluminum stock and rubber slithers. Each slither was glued onto the aluminum with a specific adhesive and allowed to set.

Adhesive	Adhering Strength
Locktite Brand Quicktite	Very Strong
Best Test Brand Rubber Cement	Moderate
Hammer Head America Brand Epoxy Cement	Low

It was apparent from this test that Loctite Brand Quicktite™ superglue was the best adhesive to utilize. To further alleviate the rubber separation problem a new U-channel rubber sole was installed. The U-channel rubber sole (see figure 13) offered more surface area for adhesion and more support against the ensuing forces of heel strike and walking.

Figure 13 – Rubber U-channel sole installed on foot

Yet another problem with the feet was the fact that despite efforts in the design stage to reduce torques on the feet to zero during a static stance, the feet were still encountered rotations about the ankle axes when in heel strike position. This was more of problem for the aft feet than the forward ones since a component of weight was directed along the aft leg placed additional torques on the aft foot causing the aft feet to have a propensity to retract to their stowed positions.

Figure 14 – Components of force directed along the walker legs that present problems when walker is in a static stance.

A possible solution to this problem is to extend the heel further rearward and further 'flatten' the sole of the foot to reduce the foot's tendency to roll along the floor when the walker is placed in a static stance. A 0.4 inch protuberance at the heel can lead to a 40-degree heel strike angle as opposed to the current 25-degree maximum heel strike angle (see figure 15).

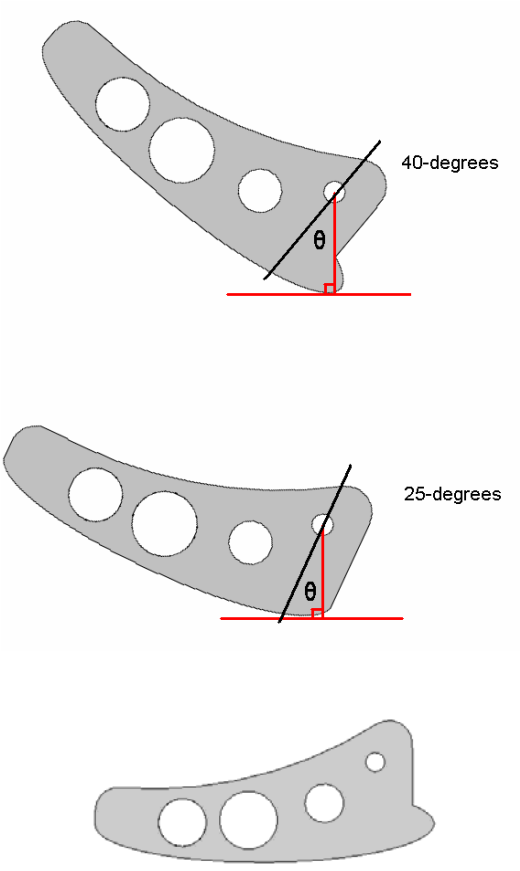

Figure 15 – Comparison of alternate foot design to current foot design.

Of course, due to increased heel length there may be scuffing issues, but this can be alleviated by retracting the foot farther backwards.

In addition to the corrections made to increase the durability of the rubber soles, there were also measures made to increase the robustness of the foot strike sensing switches. Our group had found that the original limit switches installed on the sensing feet were far too flimsy to endure prolonged walking, so subsequently the two limit switches per sensing foot were replaced with a single, more robust limit switch placed at the heel of the sensing foot.

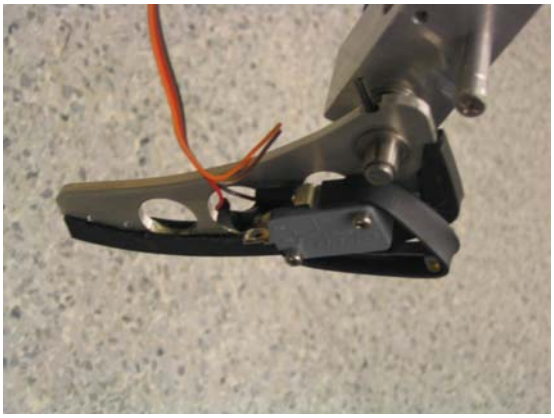

Figure 14 – Single limit switch replaces dual limit switch system. A rubber sleeve was placed over the steel lever of the switch to protect it from damage.

The toe limit switches were found to be redundant due to the accuracy of the foot position potentiometer readings, thus one can detect heel strike and calibrate the exact foot position at toe-off into the control algorithm.

3.2 Tensioners

Some interesting problems occurred upon implementation of the tensioners on the walker. Upon their initial installation at the midpoint of each of the legs (see figure 16) it was found that the tensioners, even at their fully extended positions could not provide adequate tension on the foot actuating belts. During the sudden shock of heel strike, the belt sprockets would skip notches. This was an incredibly disastrous outcome because if the sprockets skipped notches on the belt, the potentiometer readings would become inaccurate, and consequently the foot positions during each phase of walking would be erroneous. The solution to this problem, in retrospect was simple. To increase the tension in the foot actuation belts without fully extending the tensioners required that the tensioners be placed closer to the primary belt sprockets.

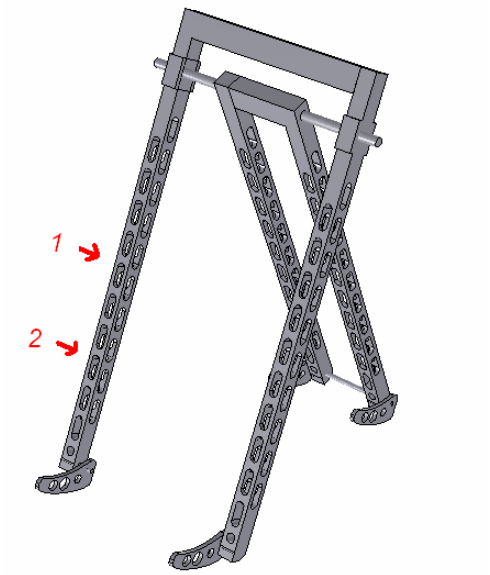

Figure 16 – Position of tensioners. (1) The original tensioner position, (2) the current tensioner position.

There are six primary belt sprockets in total and their function is to transfer toques from the motors, via the belts, to the feet (see figure 17). These sprockets are located above the walker's hip and at the ankle shafts.

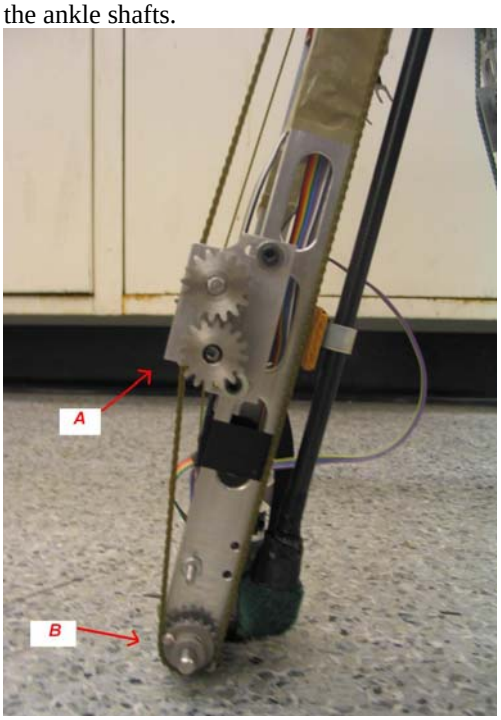

Figure 17 – (A) Tensioner, (B) one of six primary belt sprockets.

Due to spatial constraints, however, the tensioners could only be moved lower down the legs towards the belt ankle sprockets (see figure 16).

4 Conclusion

At the conclusion of this semester's marathon walker project it was duly noted that the iterative design process is both necessary and ongoing. Presumably the most ideal design is converged upon with each step of the process. Further refinement of the feet is necessary to counter the lingering problems discussed, however the current feet do not impede walking. The feet have fulfilled part of the outset objectives by being robust and functional. Efficiency will be achieved by optimizing the alternative design discussed in Section 3.1 of this report. The tensioner design, as previously mentioned, exhibited an excellent combination of durability, adjustability and maintainability over the most prominent alternative design. Unfortunately, the walker itself, was unable to achieve the outset goal of a mile of continuous walking. In fact, it was only able to make three un-assisted steps during the testing period. However, those three unassisted steps hold great promise that further adjustment of the mechanical systems and software can produce very positive results with time.

Acknowledgements

I am highly grateful of the critiquing that my colleagues at the BioRobotics and Locomotion Laboratory placed upon the designs discussed in this report. I especially would like to thank Gregg Stiesberg, Matthew Haberland, Michael Sherback and Christopher Cheng for their valuable input in improving the discussed designs. Thanks are also in order for William Seidel and Matthew Strasberg who read and revised iterations of this report. Lastly, but not in the least, I would like to extend my sincere gratitude to Professor Andy Ruina for his overall encouragement, theoretical advice, and his uninhibited patronage and generosity.

References

Yevmenenko, Y. 2000. Powered Straight Legged Walker with Circular Feet. *Masters of Engineering Thesis*. T&AM, Cornell University

Yeshua, O. 2003. Power & Control of a 2D Passive-Dynamic Walking Robot. *M&AE 490 Final Paper*. T&AM, Cornell Univerisity.

Baumeister, T., Avallone, E., Baumeister III, T. Marks' Standard Handbook for Mechanical Engineers 8th Edition. McGraw Hill 1979.

Beer, F., Johnston, R. Mechanics of Materials 2nd Edition. McGraw Hill 1992.

Appendix

Initial foot design concept:

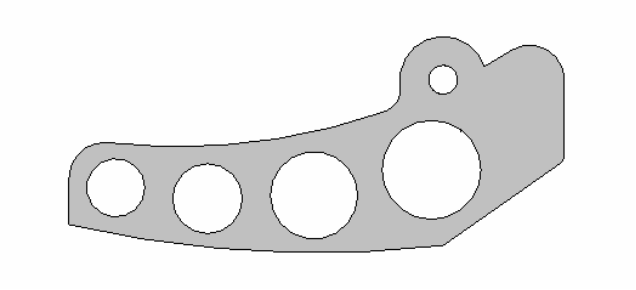

Iteration #2

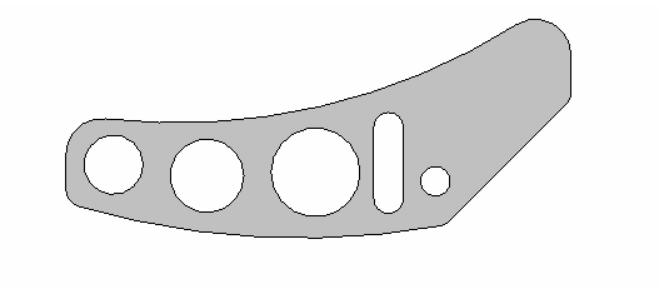

Iteration #3

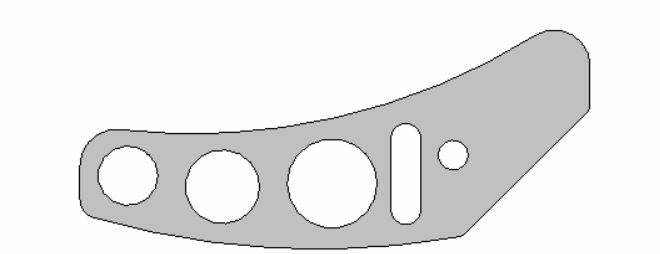

These concepts were abandoned because heel strike would effectively occur at a sharp corner. This was not desirable because foot impact on a sharp edge can damage the contact surface and form undue concentrated stresses at that small point on the foot. Additionally, design iterations 2 and 3 had large protuberances aft of the ankle axis which can scuff while the foot moves during walking.

Engineering Drawings:

Final Foot Design:

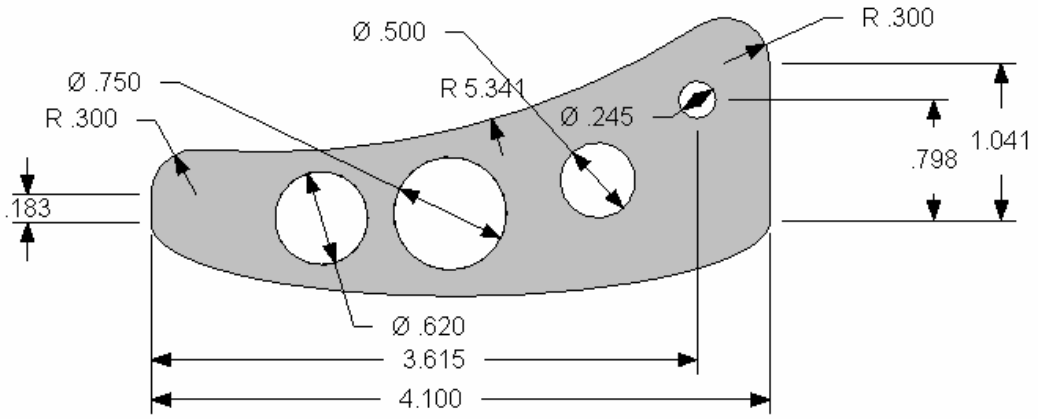

Final Tensioner Design:

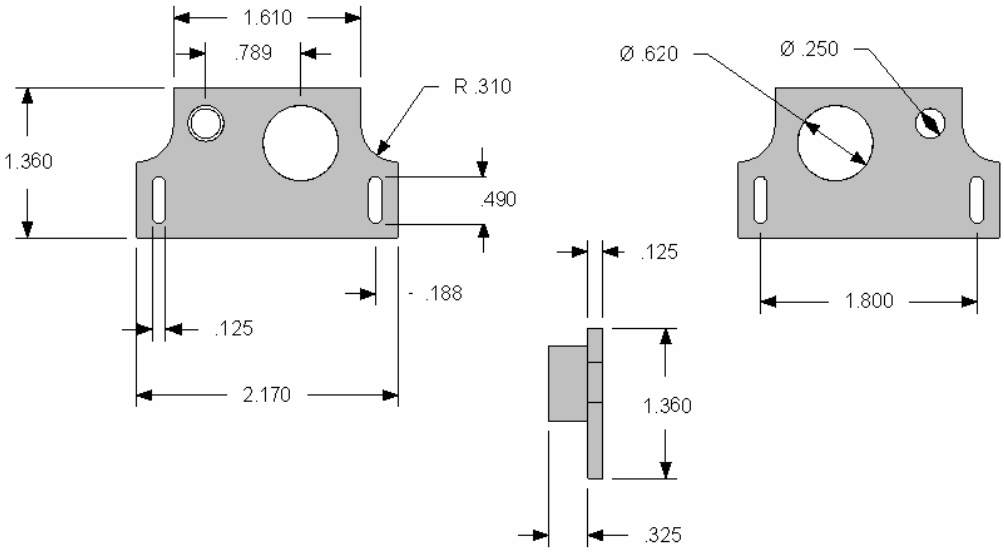

Bill of Parts

Component	Manufacturer	Quantity	Part Number
Shielded Ball Bearings	WM Berg	6	B2-11-S-Q3
Aluminum Chain Sprocket	WM Berg	3	14LC164A-18
Stainless Steel Clamps	WM Berg	4	CG1-12
Precision Spur Gears [16 teeth]	WM Berg	4	P20S28-16
Annealed Steel Cylindrical Stock (0.25-inch dia)[10inches]	Clark Hall Stock Room	1	-
3/32-inch spring pin	Clark Hall Stock Room	4	-
U-Channel Rubber Stock	McMaster-Carr	4-ft	-

Aluminum Chain Sprockets

3.75 mm (Nominal) Circular Pitch Aluminum Din 3.1355 Gold Anodized

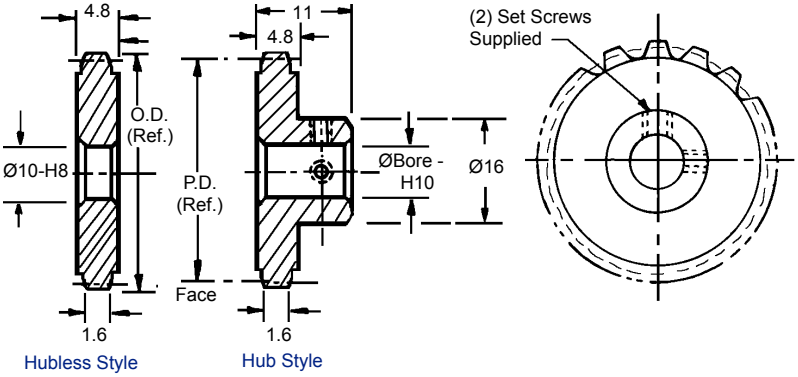

Operates with FLEX-E-PITCH® Chain 14CCF Series

HUBLESS STYLE	HUB STYLE					
Ø10 BORE	Ø4 BORE	Ø6 BORE	Ø8 BORE	NO. OF TEETH	PITCH DIAMETER	OUTSIDE DIAMETER
STOCK NO.	STOCK NO.	STOCK NO.	STOCK NO.			
–	14LC165A-13	14LC164A-13	14LC263A-13	13*	15.60•	17.63
14LP176A-14	14LC165A-14	14LC164A-14	14LC263A-14	14*	16.80•	18.82
14LP176A-15	14LC165A-15	14LC164A-15	14LC263A-15	15	18.00•	20.03
14LP176A-16	14LC165A-16	14LC164A-16	14LC263A-16	16	19.20•	21.23
14LP176A-18	14LC165A-18	14LC164A-18	14LC263A-18	18	21.60	23.63
14LP176A-20	14LC165A-20	14LC164A-20	14LC263A-20	20	24.00	26.03
14LP176A-24	14LC165A-24	14LC164A-24	14LC263A-24	24	28.80	30.83
14LP176A-25	14LC165A-25	14LC164A-25	14LC263A-25	25	30.00	32.03
14LP176A-27	14LC165A-27	14LC164A-27	14LC263A-27	27	32.40	34.43
14LP176A-28	14LC165A-28	14LC164A-28	14LC263A-28	28	33.60	35.63
14LP176A-29	14LC165A-29	14LC164A-29	14LC263A-29	29	34.80	36.83
14LP176A-30	14LC165A-30	14LC164A-30	14LC263A-30	30	35.99	38.03
14LP176A-32	14LC165A-32	14LC164A-32	14LC263A-32	32	38.39	40.43
14LP176A-34	14LC165A-34	14LC164A-34	14LC263A-34	34	40.79	42.83
14LP176A-36	14LC165A-36	14LC164A-36	14LC263A-36	36	43.19	45.23
14LP176A-38	14LC165A-38	14LC164A-38	14LC263A-38	38	45.59	47.63
14LP176A-40	14LC165A-40	14LC164A-40	14LC263A-40	40	47.99	50.03
14LP176A-42	14LC165A-42	14LC164A-42	14LC263A-42	42	50.39	52.42
14LP176A-44	14LC165A-44	14LC164A-44	14LC263A-44	44	52.79	54.82
14LP176A-48	14LC165A-48	14LC164A-48	14LC263A-48	48	57.59	59.62
14LP176A-50	14LC165A-50	14LC164A-50	14LC263A-50	50	59.99	62.02
14LP176A-52	14LC165A-52	14LC164A-52	14LC263A-52	52	62.39	64.42
14LP176A-54	14LC165A-54	14LC164A-54	14LC263A-54	54	64.79	66.82
14LP176A-56	14LC165A-56	14LC164A-56	14LC263A-56	56	67.19	69.22
14LP176A-60	14LC165A-60	14LC164A-60	14LC263A-60	60	71.99	74.02
14LP176A-65	14LC165A-65	14LC164A-65	14LC263A-65	65	77.99	80.02
14LP176A-70	14LC165A-70	14LC164A-70	14LC263A-70	70	83.99	86.02
14LP176A-80	14LC165A-80	14LC164A-80	14LC263A-80	80	95.99	98.02

- **Sprockets Ø19.0mm P.D. and smaller for idler use only.**
  Other numbers of teeth available on request.

* **Gear teeth run out on to hub.**
Stainless Steel equivalent available.

Split Hub Clamps

Compact Design
303 Stainless Steel and Aluminum Anodized

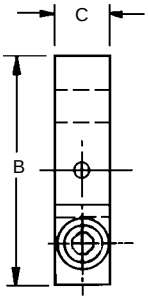

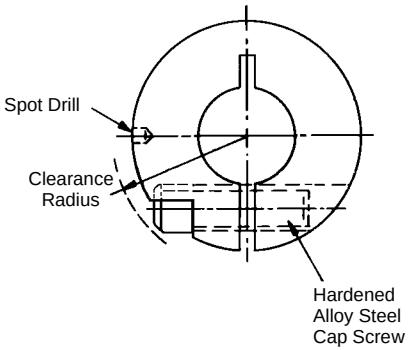

Type X

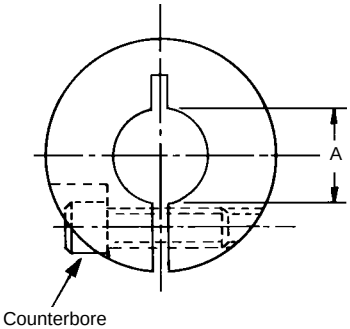

Type Z

STAINLESS STOCK NUMBER	ALUMINUM STOCK NUMBER	A DIA.	B DIA.	C	CLEAR. RADIUS	CAP SCREW THREAD	SPOT DRILL DIA.	TYPE	SPLIT HUB I.D. Ref.
CG1-1	CG1-1-A	.103	1/2	5/32	5/16	#3-48	1/16	X	---
CG1-2	CG1-2-A.	.125	1/2	5/32	5/16	#3-48	1/16	X	---
CG1-20	CG1-20-A	.125	9/16	5/32	3/8	#2-56	----	Z	---
CG1-21	CG1-21-A	.125	5/8	5/32	3/8	#2-56	----	Z	---
CG1-3	CG1-3-A	.141	1/2	5/32	5/16	#3-48	1/16	X	---
CG1-22	CG1-22-A	.188	9/16	1/8	3/8	#1-72	----	Z	5/64 TO 1/8
CG1-23	CG1-23-A	.188	9/16	5/32	3/8	#2-56	----	Z	
CG1-4	CG1-24-A	.188	5/8	5/32	11/32	#2-56	----	Z	
CG1-5	----	.188	5/8	3/16	3/8	#4-40	1/16	X	
CG1-25	CG1-25-A	.188	7/8	1/4	33/64	#6-32	----	Z	
CG1-6	----	.219	5/8	5/32	11/32	#2-56	1/16	X	---
CG1-26	CG1-26-A	.250	9/16	1/8	3/8	#1-72	----	Z	5/32 & 3/16
CG1-27	CG1-27-A	.250	9/16	5/32	3/8	#2-56	----	Z	
CG1-28	CG1-28-A	.250	5/8	5/32	3/8	#2-56	----	Z	
CG1-8	CG1-8-A	.250	7/8	3/16	31/64	#4-40	1/8	X	
CG1-9	CG1-9-A	.250	7/8	1/4	33/64	#6-32	----	Z	
CG1-10	----	.281	7/8	1/4	33/64	#6-32	1/8	X	---
CG1-11		.312	7/8	3/16	31/64	#4-40	1/8	X	.2405 & 1/4
CG1-12	CG1-12-A	.312	7/8	1/4	33/64	#6-32	----	Z	
CG1-14	CG1-14-A	.375	1-1/8	1/4	21/32	#8-32	3/16	X	5/16
CG1-15	CG1-15-A	.375	1-1/4	5/16	11/16	#8-32	----	Z	
CG1-31	----	.375	1-1/4	5/16	5/8	#8-32	----	Z	
CG1-17	CG1-17-A	.437	1-1/8	1/4	21/32	#8-32	3/16	X	3/8
CG1-18	CG1-18-A	.437	1-1/4	5/16	11/16	#8-32	----	Z	
CG1-32	----	.437	1-1/4	5/16	5/8	#8-32	----	Z	
CG1-19	CG1-19-A	.562	1-1/4	5/16	11/16	#8-32	----	Z	1/2
CG1-33	----	.562	1-1/4	5/16	5/8	#8-32	----	Z	

Special clamps are available on request

Ball Bearings

Precision ABEC-3 and ABEC-7 3/64" to 1/2" and 4mm to 8mm Bore
440C Stainless Steel Single Row Flanged

See pages K23 and K24 for bearing tolerances

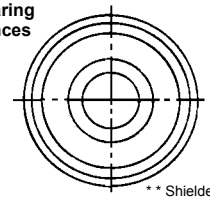

* * Shielded
Grease Per Mil-G-23827

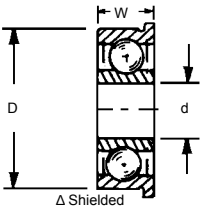

Δ Shielded
Oil Per Mil-L-6085

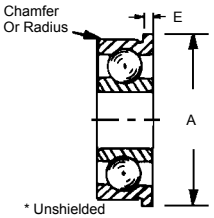

* Unshielded
Oil Per Mil-L-6085

ABEC-3 STOCK NUMBER	ABEC-7 STOCK NUMBER	ULTRA-PRECISION ABEC-7 STOCK NUMBER	d	D	W	A	SHIELD & LUBE DATA	E	DYNAMIC LOADS (LBS.) CAPACITY	STATIC LOADS (LBS.) CAPACITY
B2-16-Q3 B2-16-S-Q3	B2-16 B2-16-S	B2-16-U B2-16-S-U	.0469	.1562	.0625 .0937	.203	* * *	.013 .031	17	6
B2-17-Q3 B2-17-S-Q3	B2-17 B2-17-S	B2-17-U B2-17-S-U	.0550	.1875	.0781 .1094	.234	* * *	.023 .031	26	9
B2-12-Q3 B2-12-S-Q3	B2-12 B2-12-S	B2-12-U B2-12-S-U	.0781	.2500	.0937 .1406	.296	* * *	.023 .031	36	14
B2-13-Q3 B2-13-S-Q3	B2-13 B2-13-S	B2-13-U B2-13-S-U	.1250	.3125	.1094 .1406	.359	* * *	.023 .031	60	24
B2-14-Q3 B2-14-S-Q3	B2-14 B2-14-S	B2-14-U B2-14-S-U		.2500	.0937 .1094	.296	* * *	.023 .031	33	13
B2-15-Q3 B2-15-S-Q3	B2-15 B2-15-S	B2-15-U B2-15-S-U		.3125	.1094 .1406	.359	* * *	.023 .031	60	24
B2-5-Q3 B2-5S-Q3	B2-5 B2-5S	B2-5-U B2-5S-U		.3750	.1562 .1562	.440	* * *	.030 .030	68	28
B2-20-Q3 B2-20-S-Q3	B2-20 B2-20-S	B2-20-U B2-20-S-U	.1562	.3125	.1094 .1250	.359	* * *	.023 .036	33	14
B2-18-Q3 B2-18-S-Q3	B2-18 B2-18-S	B2-18-U B2-18-S-U	.1875	.3125	.1094 .1250	.359	* * *	.023 .036	33	14
B2-9-Q3 B2-9-S-Q3	B2-9 B2-9-S	B2-9-U B2-9-S-U		.3750	.1250 .1250	.422	* * *	.023 .031	76	33
B2-6-Q3 B2-6-S-Q3	B2-6 B2-6-S	B2-6-U B2-6-S-U		.5000	.1562 .1960	.565	* * *	.042 .042	141	67
B2-10-Q3 B2-10-S-Q3	B2-10 B2-10-S	B2-10-U B2-10-S-U	.2500	.3750	.1250 .1250	.422	* * *	.023 .036	37	
B2-11-Q3 B2-11-S-Q3	B2-11 B2-11-S	B2-11-U B2-11-S-U		.5000	.1250 .1875	.547	* * *	.023 .045	114	57
B2-7-Q3 B2-7-S-Q3	B2-7 B2-7-S	B2-7-U B2-7-S-U		.6250	.1960 .1960	.690	* * *	.042 .042	158	78
B2-21-Q3 B2-21-S-Q3	B2-21 B2-21-S	B2-21-U B2-21-S-U	.3125	.5000	.1562 .1562	.547	* * *	.031 .031	56	31
B2-8-Q3 B2-8-S-Q3	B2-8 B2-8-S	B2-8-U B2-8-S-U	.3750	.8750	.2812 .2812	.969	* * *	.062 .062	356	176
B2-22-S-Q3	B2-22-S	B2-22-S-U	.5000	1.1250	.3125	1.225	* *	.062	827	464

Metric Ball Bearing

STOCK NUMBER	d (INCHES) mm	D (INCHES) mm	W mm	A (INCHES) mm	SHIELD & LUBE DATA	E mm	DYNAMIC LOAD	STATIC LOADS
B2-104-7 B2-104-S-7	(.1575) 4,0	(.3543) 9,0	2,5 4,0	(.405) 10,3	* Δ	0,60 1,00	68	28
B2-106-7 B2-106-S-7	(.2362) 6,0	(.5118) 13,0	3,5 5,0	(.590) 15,0	* Δ	1,00 1,10	114	57
B2-108-7 B2-108-S-7	(.3150) 8,0	(.6299) 16,0	4,0 6,0	(.708) 18,0	* Δ	1,00 1,30	181	85

Additional metric sizes available from stock. Bore tolerance for Ultra Precision -.0001 / -.0002.

Precision Spur Gears

20 Pitch 1/4" Bore 3/16" Face AGMA Quality 10
Pin Style Hub 20° Pressure Angle

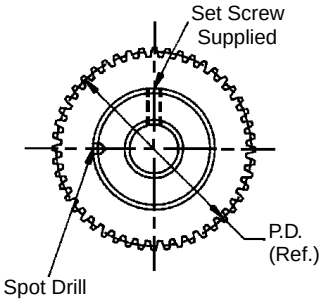

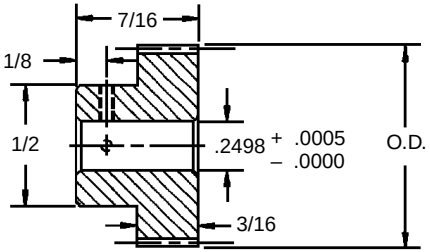

303 STAINLESS STEEL	BERG QUALITY #10 OR BETTER PER AGMA STANDARD 2000-A88		
STOCK NUMBER	NO. OF TEETH	PITCH DIAMETER	OUTSIDE DIAMETER
P20S28-14	14▲	.7000	.800
P20S28-15	15▲	.7500	.850
P20S28-16	16▲	.8000	.900
P20S28-18	18	.9000	1.000
P20S28-20	20	1.0000	1.100
P20S28-24	24	1.2000	1.300
P20S28-25	25	1.2500	1.350
P20S28-30	30	1.5000	1.600
P20S28-40	40	2.0000	2.100
P20S28-50	50	2.5000	2.600
P20S28-60	60	3.0000	3.100
P20S28-70	70	3.5000	3.600
P20S28-80	80	4.0000	4.100

▲ Hub diameter never exceeds root diameter of gear.

Available On Request:Other Numbers of Teeth;
14-1/2° Pressure Angle.